INTERNATIONAL SOCIETY FOR
SOIL MECHANICS AND
GEOTECHNICAL ENGINEERING

This paper was downloaded from the Online Library of the International Society for Soil Mechanics and Geotechnical Engineering (ISSMGE). The library is available here:

https://www.issmge.org/publications/online-library

This is an open-access database that archives thousands of papers published under the Auspices of the ISSMGE.

The paper was published in the proceedings of the 11th International Conference on Physical Modelling in Geotechnics (ICPMG2026) and was edited by Ioannis Anastasopoulos. The conference was held from June 8th to June 12th 2026 in Zurich, Switzerland.

© 2026 the Authors

Effects of unconfined compressive strength and breakage on the bearing capacity of rubble mounds: Insights from laboratory and DEM investigations

R. Sukhumkitcharoen
Port and Airport Research Institute, Yokosuka, Japan, sukhumkitcharoen@p.mpat.go.jp

I. Sato, M. Otsubo, and O. Kurihara
Port and Airport Research Institute, Yokosuka, Japan,
satoh-i-p@p.mpat.go.jp, otsubo-m@p.mpat.go.jp, kurihara-oo@p.mpat.go.jp

H. Takahashi
Tokyo University of Marine Science and Technology, Tokyo, Japan, takahashi-h@kaiyodai.ac.jp

ABSTRACT: Due to the rising cost of high-quality rock in Japan, the use of materials with lower unconfined compressive strength (UCS) than those specified in the standard for rubble mound structures is gaining increased attention. To ensure their safe application, it is essential to understand how stone characteristics, particularly strength and crushability, influence the overall bearing capacity. This study presents centrifuge model experiments on standing mounds constructed from two rock types with different UCS values, together with discrete element method simulations of a benchmark rubble mound composed of bonded particles representing eight different UCS levels, to evaluate bearing capacity and investigate particle breakage behaviour. The results indicate that, up to maximum stress levels of 300 kPa, both materials exhibited quite similar bearing capacity despite about threefold difference in UCS. It is due to the bearing capacity being insensitive to UCS under limited particle breakage at low stress levels, whereas a pronounced nonlinear dependence on UCS emerges once UCS drops below a critical threshold associated with extensive breakage at high stresses. These findings highlight the importance of considering breakage effects across different stress levels when evaluating the physical and mechanical performance of structures composed of crushable materials.

1 INTRODUCTION

A rubble mound is a common foundation for port and harbour structures such as breakwater caissons. According to Mohr-Coulomb's law and slope stability analysis, the bearing capacity is primarily governed and determined by the shear strength parameters: apparent cohesion (c) and friction angle (ϕ). Estimating these parameters from unconfined compressive strength (UCS) has been widely adopted as an alternative to costly large-scale triaxial testing of rock materials (Piratheepan et al., 2012; Sivakugan et al., 2014; Xie et al., 2025). However, establishing reliable correlations for design and ensuring proper control of material specifications on site are essential to prevent potential failure.

In Japan, it is customary to use stone with a UCS of 49.1 MPa or higher, categorized as hard stone according to the Japanese Industrial Standard (JIS), which serves as the material standard commonly adopted in the market. As high-quality rock becomes increasingly expensive, the use of lower-strength materials has become inevitable. At the same time, some reports (e.g., Kobayashi et al., 1987) indicate that slightly weaker rock can still provide sufficient shear strength, suggesting the need to investigate which types of rock can be effectively utilized. This highlights the importance of a deeper understanding of how UCS influences bearing capacity to ensure safe and reliable design.

Researchers have reported various correlations between UCS and bearing capacity, ranging from linear (Rowe and Armitage, 1987; Le Tirant, 1992) to nonlinear or power-law forms (Zhang and Einstein, 1998; Vipulanandan et al., 2007). Although most findings are derived from pile foundations, the same mechanisms are considered applicable to caissons. Furthermore, particle breakage is recognized as a dominant factor; materials with lower UCS exhibit greater crushability under stress, leading to reduced shear strength parameters and diminished bearing performance (Yu, 2017; Kahraman et al., 2018). However, quantitative studies on how these microscopic characteristics govern macroscopic behaviour are still limited.

In this study, the correlation of the behaviour of rubble materials across two laboratory scales is examined: micro-scale (unconfined compression test, represented by UCS) and macro-scale (centrifuge model test, represented by bearing capacity). A breakage analysis is also conducted to clarify the role of particle breakage in governing the global response. In addition, a preliminary DEM simulation using the bonded particle model (BPM) is performed to provide qualitative insight into the experimental behaviour and to examine the associated micromechanical mechanisms. An overview of this study is illustrated in Fig. 1.

2 CENTRIFUGE MODEL TEST

2.1 Materials

Two rubble materials (as denoted in Fig. 2), obtained as by-products from debris flows of Mount Fuji, Japan, were used in this study, and their properties are summarized in Table 1. Based on physical characteristics such as apparent specific gravity, water absorption, and visual observation, rock type 2 appears more porous, which likely contributes to its lower mechanical performance in terms of Young's modulus and UCS.

Although the cores of two diameters (0.05 m and 0.10 m) were selected randomly, a significant difference in the average UCS was observed between the two rock types, with rock type 2 showing approximately three times lower strength than rock type 1. As shown in the UCS frequency distributions in Fig. 3, about 25 % of rock type 2 is classified as non-hard rock according to the JIS standard. Although the average UCS of rock type 2 exceeds 50 MPa, the inclusion of lower-strength portions categorizes it as a low-quality material.

The particle size distribution (PSD) used in the model tests is presented in Fig. 4. The particle diameter is within the range of 4.75–9.50 mm, and the median particle size (D_{50}) is 7.13 mm, which corresponds to 0.36 m at the prototype scale under 50G.

Table 1. Summary of testing materials' properties

Properties	Type1	Type2
Apparent specific gravity (kg/m^3)	2730	2290
Water absorption (%)	1.18	3.83
Young's Modulus, E_{50} (GPa)	28.1	21.9
UCS (MPa)	>181.6*	65.7

*The UCS of one specimen exceeded the load cell capacity; the reported value therefore represents a lower bound of the average UCS.

2.2 Testing apparatus

The Hydro-Geotechnical Centrifuge PARI Mark II-R with an effective radius of 3.8 m, capable of 113g maximum acceleration and a payload of 2,710 kg, was employed to conduct bearing capacity test of rubble mound. Further details on the apparatus can be found in the technical report by Takahashi et al. (2019).

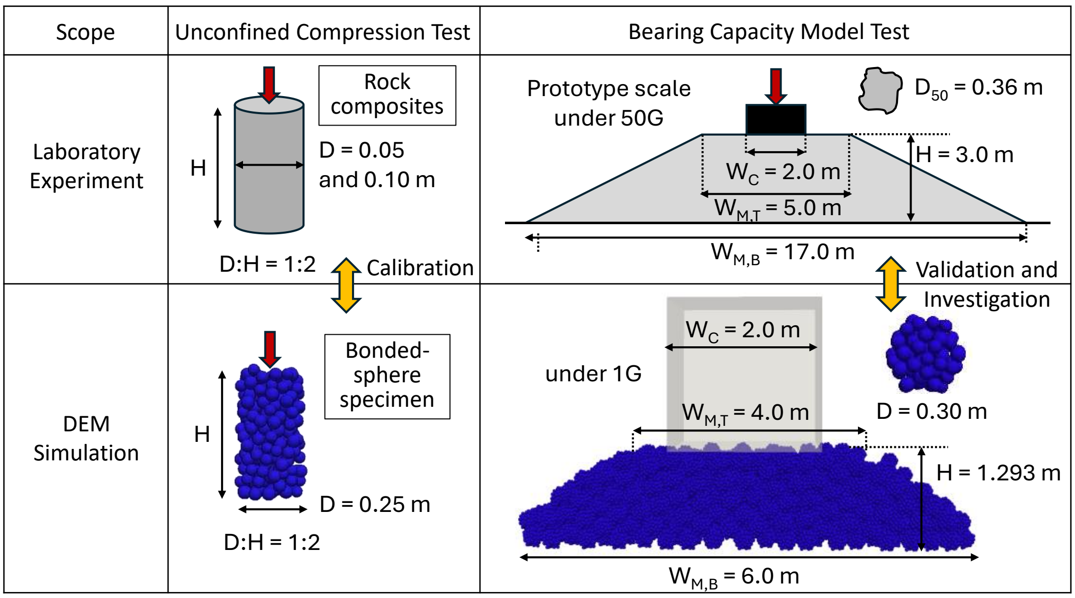

Figure 1. Overview of this study

Figure 2. Images of two rock types

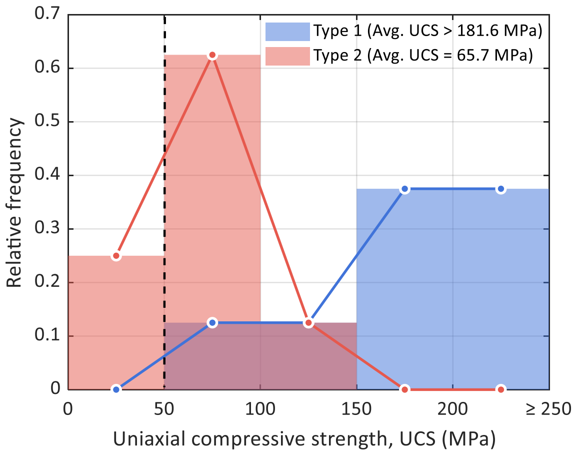

Figure 3. Frequency distributions of UCS in two rock types

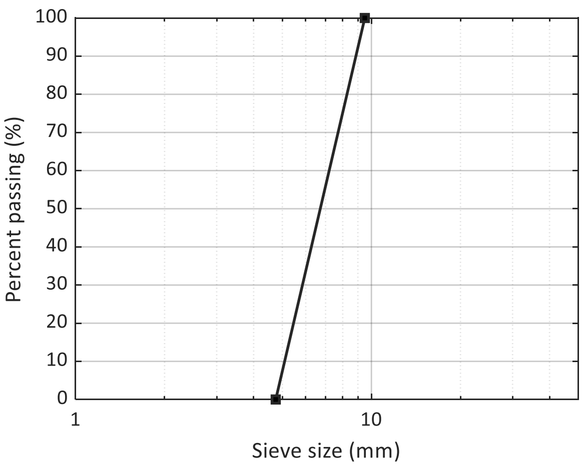

Figure 4. Particle size distribution in centrifuge model test

2.3 Testing procedure

The bearing capacity model, consisting of a mound and a caisson, was prepared in a rigid metal container having a thickness of 0.15 m perpendicular to the x–z plane. The mound was constructed entirely of a single rock type, forming a trapezoidal cross-section with a slope of 1:2 as denoted in Fig. 1. Its top width, bottom width, and height were 0.10 m, 0.34 m, and 0.06 m, respectively, corresponding to prototype dimensions of 5 × 17 × 3 m under a 50g acceleration field. A metal plate was used to represent the caisson as a simplified physical model, with a mass equivalent to that of the concrete–sand mixed caisson, having a cross-section of 0.04 × 0.08 m (equivalent to 2 × 4 m at the prototype scale).

After model preparation, the centrifugal acceleration was gradually increased from 1g to 50 g. Once the target acceleration was reached, vertical loading was applied at the center of the caisson plate using a hydraulic jack-type loading system (Takahashi, 2021) consisting of a loading shaft, load cell, and motor. Loading was carried out at a constant displacement rate of 0.242 mm/min.

3 MODEL TESTING‘S RESULTS

3.1 Effect of UCS on mechanical behaviour of rubble materials

Figure 5 illustrates the bearing capacities of the two rock types obtained from the centrifuge model tests. By evaluating the settlement of the mound under a statically placed caisson, it was observed that the two rock types exhibit nearly identical displacements up to an applied vertical stress of about 300 kPa, corresponding to caissons approximately 15 m in height. However, a greater degree of settlement and an overall reduction in stability for rock type 2 were observed as the stress level increased, becoming noticeable at around 500 kPa and pronounced at 1000 kPa, where up to a 50% increase in settlement and about a 25% reduction in bearing capacity at equivalent displacements were recorded. This suggests that the significant lower UCS of rock type 2 does not significantly affect bearing capacity at low stress levels but becomes critical at higher stress levels. Further investigation is required to clarify the mechanisms governing this behaviour.

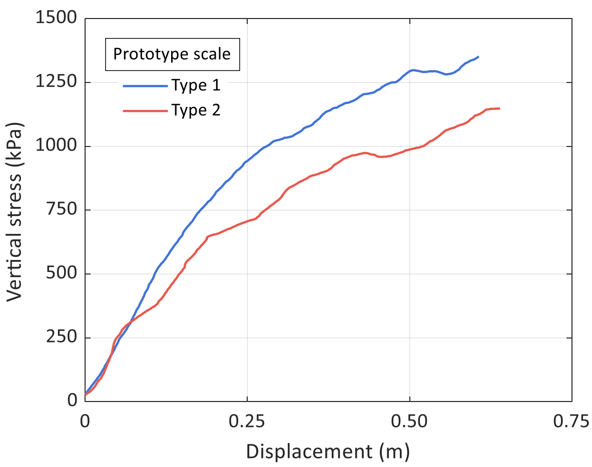

Figure 5. Relationships between applied vertical stress and displacement of caisson in bearing capacity tests

3.2 Particle breakage characteristics

The sieve analysis results before and after the model tests are presented in Fig. 6. Although the PSD considering the overall rock volume beneath the caisson (from top to bottom, denoted by the circle) shows only minor change at the end of the centrifuge test, the region subjected to stress concentration, particularly near the boundary (approximately one third from the bottom wall, denoted by the square), exhibits distinct differences between two rocks.

The more pronounced differences observed between the two rock types under higher stress levels can be attributed to increased particle breakage, which in turn enhances contractive tendencies with rising confining pressure, especially in lower-strength materials. Therefore, it can be inferred that particle breakage or crushing, corresponding to their UCS, are directly related to the reduced bearing capacity observed in rock type 2.

However, experimental testing is inherently limited by the difficulty of performing progressive sieving analyses to capture particle breakage at specific stage. The results are also affected by the complex interaction of factors such as particle density, Young's modulus, porosity, and particle shape, since controlling a single parameter, such as UCS, in isolation is challenging. To address these limitations, a complementary parametric study using a reliable numerical simulation is required to systematically assess the relationship between UCS, crushing behaviour, and bearing capacity in more analytical detail.

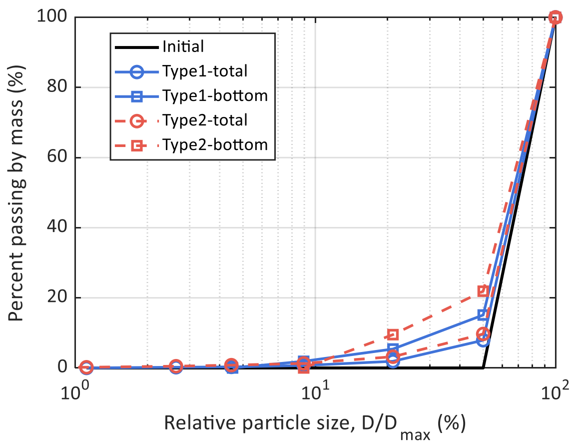

Figure 6. Particle size distributions before/after the centrifuge model tests

4 DISCRETE ELEMENT METHOD (DEM): BEARING CAPACITY SIMULATION

The numerical simulation named the discrete element method (DEM) is widely adopted for modeling rock behaviour (Irani et al., 2025) and was specifically employed in this study to simulate the bearing capacity test. The bonded particle model (BPM) (Potyondy and Cundall, 2004) implemented in the Large-scale Atomic/Molecular Massively Parallel Simulator (LAMMPS) was utilized to represent breakable clumped particles. The criterion for bond breakage is defined as

$$B = \max\left\{0, \frac{f_r}{f_{r,c}} + \frac{|f_s|}{f_{s,c}} + \frac{|\tau_b|}{\tau_{b,c}} + \frac{|\tau_t|}{\tau_{t,c}}\right\} \qquad (1)$$

where f_r and f_s are the normal and shear forces, and τ_b and τ_t are the bending and twisting torques acting on the bond, respectively. These depend on the bond stiffnesses k_r, k_s, k_b, and k_t for normal, shear, bending, and twisting modes. Meanwhile, $f_{r,c}, f_{s,c}, \tau_{b,c}$, and $\tau_{t,c}$ represent the corresponding bond strengths in each mode. A bond is considered broken when $B \geq 1$.

4.1 Calibration of input parameters

In this study, a parallel bond model was adopted, in which bonded particles interact through both pair contacts (gran/hertz/history; Hertz, 1881; Mindlin, 1949) and bond contacts (bpm/rotational; Wang, 2009). Three pair-contact parameters for silica sands and eight bond parameters were employed, as summarized in Table 2. For simplification, the four bond parameters representing the four breakage modes were assumed to be identical, and only the bond strength was varied to calibrate UCS values.

Table 2. Simulation parameters used in this study

Properties	**Parameter values**
Particle density (kg/m³)	2650
Pair contact model	gran/hertz/history
Particle shear modulus (GPa)	29.1
Poisson's ratio	0.23
Interparticle friction	0.4 (particle-particle, particle-caisson) and 0.0 (particle-wall)
Bond contact model	bpm/rotational
Bond stiffnesses, k_r, k_s, k_b, and k_t (×10⁶; N/m, N/m, N·m, N·m)	100
Bond strengths, $f_{r,c}, f_{s,c}, \tau_{b,c}$, and $\tau_{t,c}$ (×10³; N, N, N·m, N·m)	4 (L), 11 (P), 15 (M), 18.5 (J), 25 (H4), 50 (H3), 70 (H2), and 80 (H1)

A core compression simulation (denoted in Fig. 1) was then conducted on a cylindrical specimen (height 0.50 m, diameter 0.25 m) composed of spherical particles with an average diameter of approximately 0.05 m and a particle density of 2650 kg/m³. The resulting stress–strain relationships are illustrated in Fig. 7. Using rock J (49.3 MPa) as the reference material, the rock samples were categorized into higher-strength rocks, namely H1 (199.9 MPa), H2 (177.7 MPa), H3 (125.9 MPa), and H4 (67.2 MPa), and lower-strength rocks, namely M (40.4 MPa), P (29.4 MPa), and L (10.8 MPa). The E_{50} values are approximately 5 GPa for all specimens, which are lower than those reported in the experiments.

It should be noted that UCS is the primary focus of this study and has been used for the calibration and validation of the DEM model, consistent with engineering practice in which UCS is adopted as a quality control parameter prior to construction. Future research should extend the calibration and validation framework to incorporate assembly-scale characteristics, such as shear strength parameters.

The assessment of the model was further conducted through additional unconfined tension simulations. The results show a consistent unconfined tensile strength (UTS) to UCS ratio within the typical range of 0.1–0.2 reported for rock-like materials. In addition, realistic failure patterns were reproduced, including shear band formation under compression and axial splitting under tension. Despite the simplified assumption of identical bond properties for the four individual bond failure modes, the rock core assembly exhibits both quantitatively reasonable strength ratios and qualitatively realistic failure behaviour under different loading conditions.

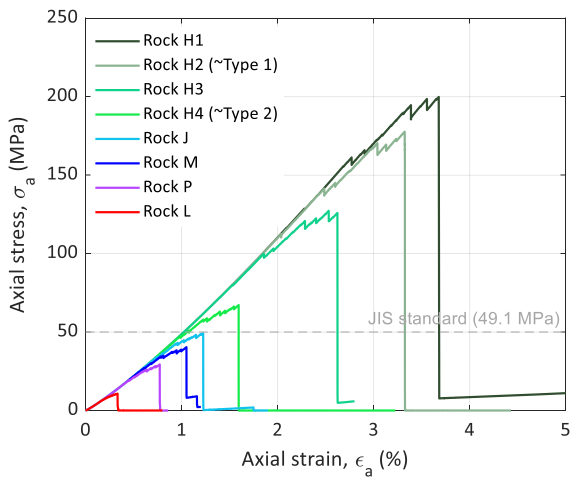

Figure 7. Stress–strain relationships from unconfined compression simulations using DEM (denoted in Fig. 1) for eight rock types

4.2 Simulation setup

Before preparing the mound model, the bonded core, initially produced at a larger size, was trimmed into a spherical shape with a diameter of 0.3 m, consisting of 80 spheres and 285 bonds.

In the first stage, spherical particles with a diameter of 0.303 m were pluviated into a rectangular box with dimensions of 6 m × 2 m in the x and y directions and an infinite extent in the z direction under gravitational acceleration of 9.81 m/s². Particles located outside the target trapezoidal region (denoted in Fig. 1) were removed, and the remaining particles were replaced with bonded particles prepared in advance to achieve the intended geometry.

A leveling process was then performed by moving the wall at the top to achieve the target height (z = 1.293 m) and ensure a smooth surface. Finally, a cubic loading block with dimensions of 2 m × 2 m × 2 m was positioned at the center of the top surface and moved downward at a loading speed of 1.5 m/s to evaluate the bearing capacity.

This relatively high loading rate is considered acceptable for neglecting inertia effects, as the kinetic-to-strain energy ratio remained sufficiently small (approximately 2–3%) at the end of all cases. Although some dynamic effects are inevitable during the initial stage of the model-scale setup due to the low confining pressure, these inertia effects become minimized as the mean stress level increases and particle breakage progresses, resulting in smaller mean particle diameters. In addition, Cundall's (1987) linear and angular damping coefficients of 0.1 were applied to dissipate kinetic energy. It should also be noted that the loading rate during actual construction is difficult to quantify and may exceed the value adopted in this study, potentially inducing more pronounced dynamic effects. Nevertheless, the quasi-static response serves as an essential basis for understanding the fundamental behaviour of the rubble mound, regardless of loading rate effects.

It should be emphasized that, at this preliminary stage, lower core stiffness and reduced model dimensions, including particle size and rubble mound geometry, were adopted in the DEM simulations compared to the experiments in order to minimize computational time, while still enabling a qualitative investigation of the effects of UCS and particle breakage, in accordance with the primary objective of this study.

5 DEM RESULTS

5.1 Effect of UCS on bearing capacity

The bearing capacity of rubble mounds constructed from eight rock types in the DEM simulations is illustrated in Fig. 8a, using consistent line colours corresponding to their UCS values. The corresponding fitting curve results are shown in Fig. 8b, together with the centrifuge test results plotted as dotted lines, using the same representative colours for rock types 1 and 2 as before. The overall behaviour of rocks H2 and H4 (indicated by the dashed fitted lines), which have UCS values comparable to rock types 1 and 2, shows good agreement with the experimental data. Both exhibit an initial rapid increase in vertical stress followed by a gradual reduction in the rate of increase, with stress levels remaining within a similar range under the current simulation conditions. This consistency indicates that the DEM results successfully reproduce the centrifuge test behaviour, confirming the validity of the numerical model as a reliable benchmark for subsequent parametric studies. It should be noted that the initial stiffness difference observed in the laboratory may not be replicated when identical material stiffness is used.

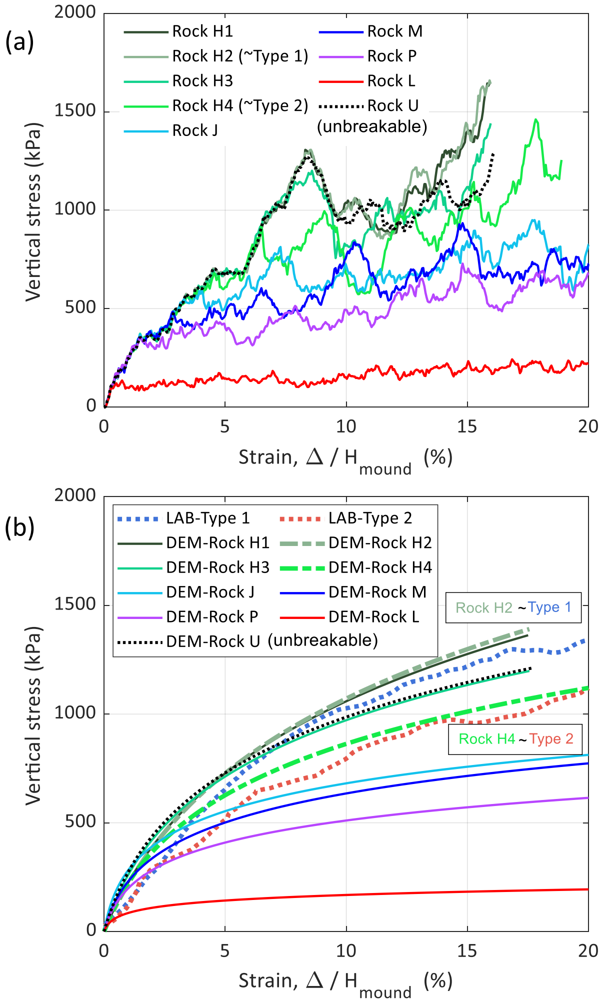

Figure 8. Stress–strain relationships from (a) bearing capacity simulations using DEM and (b) their corresponding fitting curves, compared with two experimental tests (Types 1 and 2)

It should be clarified that the comparable bearing capacity observed in the DEM simulations primarily results from the current model configuration, despite discrepancies with the laboratory (LAB) setup. In particular, the twofold difference in particle size relative to mound height (D/H = 0.23 in DEM and 0.12 in LAB) is likely more influential than the 17% difference in particle size relative to caisson width (D/W = 0.15 in DEM and 0.18 in LAB). While variations in D/W may affect load-transfer mechanisms and strain localization, the reduced mound height produces a more concentrated load-transfer network, thereby amplifying boundary effects and particle breakage. The resulting geometric constraint further limits shear band development, contributing to the relatively high bearing capacity despite the lower core stiffness. These effects may be partially moderated by the use of smaller bonded particles. Despite these limitations, the following discussion provides meaningful qualitative insight into the experimental observations and the underlying micromechanical mechanisms.

In the ideal case of rock U with infinite UCS (unbreakable material), represented by the black dotted curve in Figs. 8a and 8b, the vertical stress continues to increase with strain. In contrast, for breakable materials, the stress–strain curve deviates from this trend once a certain stress level is reached; materials with lower UCS deviate earlier, at lower stress levels, resulting in lower ultimate bearing capacity. By examining the DEM results for materials with identical stiffness but varying UCS, it can be confidently concluded that this reduction is attributed solely to UCS, as stiffness and other effects are excluded, unlike in the experiments.

From the DEM simulation results, the strain-based bearing capacity at 1%, 5%, and 15% strain and the induced vertical strain at specific stress levels of 200, 500, and 1000 kPa were plotted against UCS, as shown in Fig. 9. The results indicate that at lower strain and stress levels, the differences among materials with varying UCS are minimal. However, as the stress and strain levels increase, the relationship between bearing capacity, whether expressed in terms of stress or induced vertical strain, and UCS demonstrates a progressively nonlinear trend. For example, at 500 and 1000 kPa, materials with UCS above 50 and 125 MPa, respectively, show nearly identical settlements, while lower-strength materials exhibit exponentially higher strains. This finding provides clear evidence and explanation for the behaviour observed in Rock Types 1 and 2 in the laboratory.

By defining the critical threshold as the minimum UCS at which the induced vertical strain under a specified operational stress level becomes independent of UCS, it is evident that this threshold increases with increasing stress levels. This indicates that higher operational stresses require materials with correspondingly higher UCS to achieve comparable performance, whereas materials with lower UCS may be adequate under lower stress conditions. Therefore, the application of a universal UCS criterion for pre-construction material assessment may be inappropriate, as it could lead to either over-conservative or under-conservative design depending on the intended operational stress level.

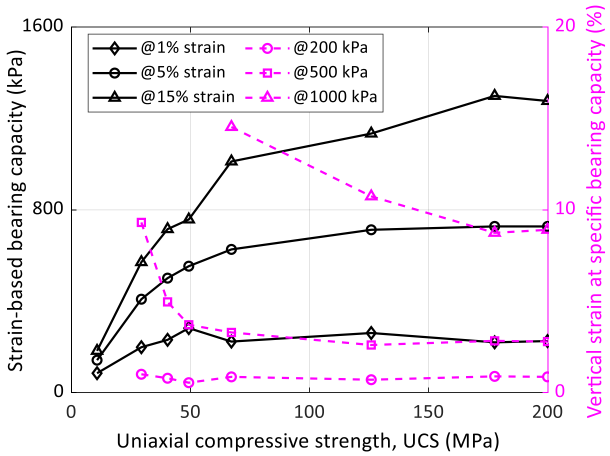

Figure 9. Relationships between bearing capacity and induced vertical strain with respect to UCS values obtained from DEM simulations

5.2 Effect of particle breakage on bearing capacity

The underlying mechanism of this phenomenon can be interpreted through the particle breakage characteristics. The number of broken bonds at each stress level for the eight materials in DEM simulations is illustrated in Fig. 10. Bond breakage is initiated earlier at lower applied stresses in materials with lower UCS, occurring at approximately 100 kPa for rock L and 800 kPa for rock H1, consistent with the inherent particle strength observed in unconfined compression tests. These materials also exhibit higher rates of particle breakage accumulation and greater number of total bond breakage at equivalent stress levels.

Such characteristics are linked to the deviations in the stress–strain curves with more gradual slopes at lower stress levels shown in Fig. 8a, where the transition occurs when roughly 500 bonds (approximately 0.25% of the total initial 199,500 bonds) are broken (around 300 kPa for rock P, 500 kPa for rock M, and 750 kPa for rock H4). Rocks H1, H2, and H3, which exhibit fewer broken bonds than this level, behave similarly to the unbreakable material, as the number of broken bonds is insufficient to affect mound stability. It is therefore implied that the reduction in bearing capacity is primarily associated with increased particle breakage, which progressively compromises the overall stability of the mound. It should be noted that the slightly higher bearing capacity observed for rocks H1 and H2 compared to the unbreakable rock at the later stage may be attributed to densification caused by the coexistence of broken and unbroken particles.

Overall, the nonlinear relationship between bearing capacity and UCS arises from the substantial accumulation of broken bonds that develop at certain stress levels. When particle breakage does not occur, or when the extent of breakage is minimal at a given stress level, the bearing capacity theoretically remains unchanged regardless of differences in UCS. In contrast, once breakage occurs, the bearing capacity decreases exponentially due to the higher rate of bond breakage development in materials with lower UCS.

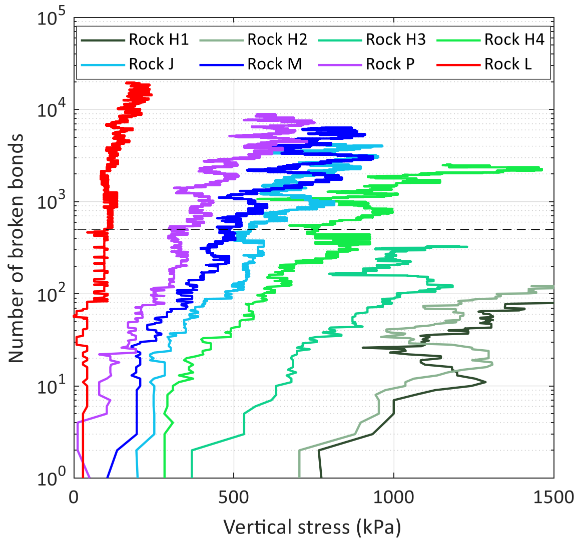

Figure 10. Relationships between the number of broken bonds and applied vertical stress obtained from DEM simulations (total initial number of bonds = 199,500)

6 CONCLUSIONS

This study investigated the influence of unconfined compressive strength (UCS) and particle breakage on the bearing capacity of rubble mounds through laboratory experiments and discrete element method (DEM) simulations. The behaviour of rock materials was examined at the particle and model levels, providing key insights into their mechanical response. The main findings are summarized as follows:

1. Bearing capacity is governed by microscale particle behaviour in terms of UCS. A nonlinear dependence is observed at higher stress levels, where materials with UCS lower than the critical threshold exhibit an exponential reduction in bearing capacity, while the two factors appear nearly independent at low stress levels.
2. The extent of breakage is the key factor controlling the reduction in bearing capacity. The constant bearing capacity corresponds to an insufficient amount of breakage, while the pronounced nonlinearity at higher stresses results from the rapid accumulation of breakage in low-UCS materials.

The crushing characteristics should not be neglected when designing structures composed of crushable materials such as rock. A deeper understanding of their behaviour is essential for ensuring both efficiency and safety in practical applications.

ACKNOWLEDGEMENTS

This research was commissioned by the Ports and Harbours Bureau, Ministry of Land, Infrastructure, Transport and Tourism, Japan, and the support is gratefully acknowledged. The authors also thank Shimizu Port, Japan, for providing the rock materials used in the experiments.

REFERENCES

Cundall, P. A. (1987). Distinct element models, of rock and soil structure. *Analytical and computational method in engineering rock mechanics*, 129-163I.

Hertz, H. (1881). Über die Berührung fester elastischer Körper [In German]. *J reine und angewandte Mathematik*, *92*, 156.

Irani, N., Tafili, M., Salimi, M., Goudarzy, M., and Wichtmann, T. (2025). Particle Breakage: Exploring the numerical and experimental approaches in crushable soil mechanics: N. Irani et al. *Archive of Applied Mechanics*, *95*(7), 151. https://doi.org/10.1007/s00419-025-02845-0

Kahraman, S. A. İ. R., Toraman, O. Y., and Cayirli, S. (2018). Predicting the strength and brittleness of rocks from a crushability index. *Bulletin of Engineering geology and the Environment*, *77*(4), 1639-1645. https://doi.org/10.1007/s10064-017-1012-9

Kobayashi, M., Terashi, M., Takahashi, K., and Odani, H. (1987). A new method for calculating the bearing capacity for rubble mounds [In Japanese]. *Report of the Port and Harbour Research Institute*, *26*(2), 371-411.

Le Tirant, P. (1992). Design guides for offshore structures: Offshore pile design.

Mindlin, R. D. (1949). Compliance of Elastic Bodies in Contact. *Journal of Applied Mechanics*, *16*(3), 259-268. https://doi.org/10.1115/1.4009973

Piratheepan, J., Gnanendran, C. T., and Arulrajah, A. (2012). Determination of c and φ from IDT and unconfined compression testing and numerical analysis. *Journal of materials in civil engineering*, *24*(9), 1153-1164. https://doi.org/10.1061/(ASCE)MT.1943-5533.0000493

Potyondy, D. O., and Cundall, P. A. (2004). A bonded-particle model for rock. *International journal of rock mechanics and mining sciences*, *41*(8), 1329-1364. https://doi.org/10.1016/j.ijrmms.2004.09.011

Rowe, R. K., and Armitage, H. H. (1987). A design method for drilled piers in soft rock. *Canadian geotechnical journal*, *24*(1), 126-142. https://doi.org/10.1139/t87-011

Sivakugan, N., Das, B. M., Lovisa, J., and Patra, C. R. (2014). Determination of c and φ of rocks from indirect tensile strength and uniaxial compression tests. *International Journal of Geotechnical Engineering*, *8*(1), 59-65. https://doi.org/10.1179/1938636213Z.00000000053

Takahashi, H., Fujii, N., Morikawa, Y., and Takano, D. (2019). Development of hydro-geotechnical centrifuge PARI Mark II-R. *Technical Note of the Port and Airport Research Institute*, (1353), 27.

Takahashi, H. (2021). Stability of composite-type breakwaters reinforced by rubble embankment. *Soils and Foundations*, *61*(2), 318-334. https://doi.org/10.1016/j.sandf.2020.10.011

Vipulanandan, C., Hussain, A., and Usluogulari, O. (2007). Parametric study of open core-hole on the behavior of drilled shafts socketed in soft rock. In *Contemporary issues in deep foundations* (pp. 1-10). https://doi.org/10.1061/40902(221)6

Wang, Y. (2009). A new algorithm to model the dynamics of 3-D bonded rigid bodies with rotations. *Acta Geotechnica*, *4*(2), 117-127. https://doi.org/10.1007/s11440-008-0072-1

Xie, S., Lin, H., Duan, H., Yao, R., and Ma, T. (2025). A novel triaxial strength criterion for rocks based on the ultimate strength and its application. *Geoenergy Science and Engineering*, *246*, 213590. https://doi.org/10.1016/j.geoen.2024.213590

Yu, F. (2017). Particle breakage and the drained shear behavior of sands. *International Journal of Geomechanics*, *17*(8), 04017041. https://doi.org/10.1061/(ASCE)GM.1943-5622.0000919

Zhang, L., and Einstein, H. H. (1998). End bearing capacity of drilled shafts in rock. *Journal of geotechnical and geoenvironmental engineering*, *124*(7), 574-584. https://doi.org/10.1061/(ASCE)1090-0241(1998)124:7(574)